

Varying Surface Chemistries for p-Doped and n-Doped Silicon Nanocrystals and Impact on Photovoltaic Devices

Tamilselvan Velusamy,^{*†} Somak Mitra,[†] Manuel Macias-Montero,[†] Vladimir Svrcek,[‡] and Davide Mariotti[†]

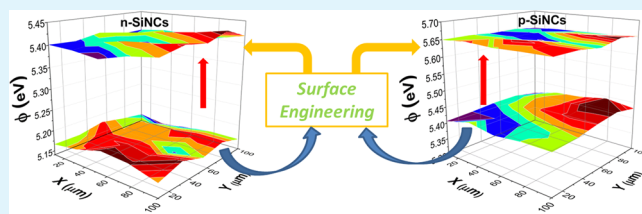
[†]Nanotechnology & Integrated Bio-Engineering Centre (NIBEC), Ulster University, Shore Road, Jordanstown BT37 0QB, U.K.

[‡]Research Center for Photovoltaics, National Institute of Advanced Industrial Science and Technology (AIST), Central 2, Umezono 1-1-1, Tsukuba, 305-8568, Japan

Supporting Information

ABSTRACT: Doping of quantum confined nanocrystals offers unique opportunities to control the bandgap and the Fermi energy level. In this contribution, boron-doped (p-doped) and phosphorus-doped (n-doped) quantum confined silicon nanocrystals (SiNCs) are surface-engineered in ethanol by an atmospheric pressure radio frequency microplasma. We reveal that surface chemistries induced on the nanocrystals strongly depend on the type of dopants and result in considerable diverse optoelectronic properties (e.g., photoluminescence quantum yield is enhanced more than 6 times for n-type SiNCs). Changes in the position of the SiNCs Fermi levels are also studied and implications for photovoltaic application are discussed.

KEYWORDS: *p/n-SiNCs, surface engineering, surface chemistry, quantum yield, Fermi level, PV device*



Fermi-level Changes of p- and n- type SiNCs Before and After Surface Engineering

INTRODUCTION

Silicon nanocrystals (SiNCs) are fascinating quantum confined structures with properties that depend on their surface characteristics and size. Surface composition and dimensions of the SiNCs can be tuned to tailor optoelectronic properties and quantum confined effects such as carrier multiplication. Silicon, the element, is also abundant and nontoxic, making it still the material of choice for many applications, including photovoltaics (PVs).^{1–6} Doping in quantum confined SiNCs is of paramount importance for SiNCs successful integration in application devices;^{4,7} however, control of the dopant density and spatial distribution remains still a challenge for many synthesis methods.^{8–11} Electrochemical etching is possibly the only approach that can reliably produce p-type and n-type SiNCs. The determination of the Fermi level can provide useful information with regard to doping and plays an important role for the band alignments of semiconductors in many applications; in particular, it determines the photocurrent collection efficiency and overall device performance of solar cells.^{12–14} The position of the Fermi level depends on dopants, physical and chemical changes of surface conditions such as crystal structure, surface roughness, adsorption layer, oxidation, and so on.^{15–17} Tuning the Fermi level of quantum confined doped SiNCs by surface engineering is therefore a powerful approach to adjust band alignment in PV devices.

In most cases, SiNCs exposure to air degrades or at least changes SiNCs properties,^{18,19} therefore a complete control on SiNCs surface characteristics is also essential for device stability.

In this context, organic passivation of SiNCs improves the stability of SiNCs properties. However, surface attachment of long organic molecules can hinder specific mechanisms; for instance, exciton dissociation within photovoltaic devices is negatively affected when organic ligands are used on the surface of SiNCs.¹⁹ Therefore, the possibility of achieving “surfactant-free” surface engineering of SiNCs is of great interest. Surface properties also determine the dispersion in colloids and distribution of SiNCs in polymeric blends, which are often used as active layer in hybrid PV devices.²⁰

Hybrid PV devices are formed by inorganic semiconducting nanocrystals embedded within a semiconducting polymeric matrix, generally assembled in a bulk-heterojunction (BHJ) architecture, which has been extensively used in the corresponding all-organic devices.^{21,22} Hybrid BHJ devices can take advantage of simple coating or printing process for fabricating the active layer, which are typical of organic devices, as well as benefit from size-dependent optical/electronic properties and carrier multiplication of the inorganic semiconducting nanocrystals.^{5,23–25}

It is therefore clear that control of surface characteristics throughout synthesis, doping and device integration of SiNCs is very important. Great progress in surface functionalization/engineering approaches has been made; however much of the

Received: July 20, 2015

Accepted: December 1, 2015



ACS Publications

© XXXX American Chemical Society

A

DOI: 10.1021/acsami.5b06577
ACS Appl. Mater. Interfaces XXXX, XXX, XXX–XXX

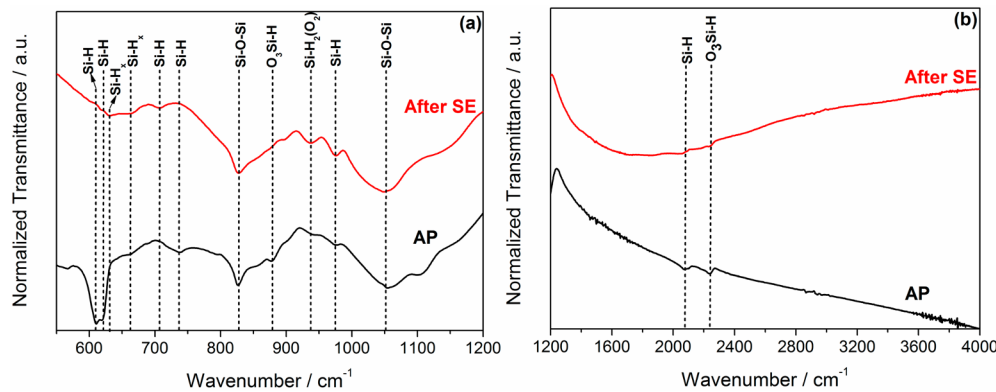


Figure 1. Fourier transform infrared (FTIR) transmission spectra of as-prepared (AP) and surface-engineered (SE) n-type silicon nanocrystals. (a) FTIR signal from 550 to 1200 cm^{-1} and (b) FTIR signal of the same samples from 1200 to 4000 cm^{-1} .

work on surface treatment of SiNCs has relied on intrinsic SiNCs, that is, with no intentional doping. Our recent studies have shown that surface engineering of electrochemically etched p-type SiNCs in liquid media by atmospheric pressure microplasma can improve the corresponding optoelectronic properties.^{4,19,26,27} However, n-type SiNCs have found very little attention in the literature; furthermore, both p-type and n-type SiNCs have not been assessed with respect to their band energy levels. It is interesting to note that also in bulk silicon PVs, boron-doped silicon (p-Si) is dominating the PV market but the 2013 edition of the International Technology Roadmap for PVs (ITRPV) states that phosphorus-doped silicon (n-Si) has the potential to compete with p-Si.^{6,28} N-Si offers some distinctive advantages compared to p-Si (e.g., boron's propensity to form defects with oxygen and greater stability of n-Si against metal impurities).^{29,30}

In this work, we have performed the surface engineering of electrochemically etched p- and n-type SiNCs. We report on how the same surface engineering process can lead to drastically different outcomes due to different doping and how this impacts the corresponding optical properties. We then report for the first time on Fermi level measurements for SiNCs and demonstrate the p- and n-type character of electrochemically etched SiNCs. Our measurements also demonstrate that surface engineering can tune the band energy levels and in particular the Fermi level. Finally we fabricate device test structure with p-/n-type SiNCs and with varying surface chemistry to demonstrate the resulting effects. In particular it is noted that band alignment, dissociation efficiency and transport are all directly affected by the interplay of varying surface chemistry and doping levels.

EXPERIMENTAL DETAILS

p-Type (boron-doped, $0.1 \Omega \text{ cm}$, thickness 0.5 mm) and n-type (phosphorus-doped, $0.1\text{--}0.5 \Omega \text{ cm}$, thickness 0.5 mm) silicon wafers are electrochemically etched to produce a porous film composed of aggregated SiNCs. The porous film is mechanically pulverized and SiNCs are then collected as powder.¹⁹ While electrochemical etching of p-type silicon wafer can be carried out in ambient conditions, electrochemical etching of n-type silicon also requires the wafer to be illuminated during the process to produce positive carriers (i.e., holes). The crystallinity, size, chemical composition, and surface characteristics of our p-type SiNCs have been extensively studied in our previous reports which included transmission electron microscopy (TEM),^{26,27} X-ray photoelectron spectroscopy (XPS)³¹ and Fourier transform spectroscopy (FTIR).^{32–34} These studies have been consistent and confirm that these SiNCs are hydrogen-terminated

for the most part, with possible dangling bonds and silicon dimers and with a degree of oxidation that depends on the storage conditions. Also the SiNCs are expected to present strong quantum confinement features as their average diameter was shown to be between 2 and 3 nm. We report in the *Supporting Information* additional material characterization for n-type SiNCs. Following, 3 mg of p-type SiNCs and 3 mg of n-type SiNCs were dispersed into separate 3.5 mL quantities of ethanol. Surface engineering of the two colloids was then carried out for 30 min using a radio frequency (RF) microplasma as in our previous work;¹⁹ corresponding control colloidal samples, referred to as as-prepared SiNCs, were also prepared, which did not undergo any surface engineering and were instead aged in ethanol for 30 min. Briefly, the RF microplasma was generated within a quartz capillary (0.7 mm internal diameter and 1 mm external diameter) and sustained by 450 MHz power at 45 W applied between ring RF/ground electrodes kept at a distance of approximately $\sim 1 \text{ mm}$. Pure argon at 150 sccm was used. The distance between the capillary end and the SiNCs/ethanol colloid was maintained at about 1 mm.

Room temperature photoluminescence with 350 nm excitation wavelength (Horiba Jobin Yvon Spectrofluorometer-Fluoromax-4) and ultraviolet-visible absorption (UV-vis; PerkinElmer Lambda 35) spectra of as-prepared (AP) and surface-engineered (SE) p- and n-type colloidal SiNCs were recorded. The surface chemistry of all samples was studied by Fourier transform infrared spectroscopy (FTIR, PerkinElmer Spectrum 2000). For these measurements, SiNCs/ethanol colloids were drop-casted on silicon substrates and allowed them to dry in atmosphere. Quantum yield measurements (Horiba Scientific QY system-Horiba Jobin Yvon Spectrofluorometer-Fluoromax-4) were taken from samples, which were drop-casted and dried on quartz substrates (*Supporting Information*). Kelvin probe (KP) measurements (SKP Kelvin Probe Version Delta 5⁺, Version 5.05 from KP Technology Ltd, U.K.) were performed to determine the Fermi energy levels of the SiNCs. The technique measures the contact potential difference (CPD) between the sample surface and a vibrating tip.¹⁵ Full details on the working principles of KP measurements are reported elsewhere^{13,16} (see also *Supporting Information*). For KP measurements, AP- and SE-SiNCs colloids were drop-casted on glass substrates which had an indium-tin-oxide (ITO) coating; the ITO layer was connected to ground during measurements. For comparison, we have also measured the Fermi level of the electrochemically etched wafers with the porous film still attached to the substrate, that is, before producing the SiNCs powder by mechanical pulverization; in this case, the silicon wafer was grounded directly.

To evaluate the impact of doping and surface engineering, we have fabricated photovoltaic device test structures with p-type and n-type AP- and SE-SiNCs. Each one of the SiNCs colloid sample was used to produce the corresponding devices. A poly(3,4-ethylenedioxothiophene) doped by poly(styrenesulfonate) (PEDOT:PSS) filtered solution was spin coated on O_2 plasma-cleaned ITO-patterned glass substrates and annealed at 135°C for 15 min. Then, 8 mg of polythieno[3,4-*b*]thiophenebenzodithiophene (PTB7) polymer is

dissolved into 3.5 mL of chlorobenzene and mechanically agitated for one night. SiNCs were first dried inside a fume hood, and then 5.4 mg of SiNCs was mixed with 3.5 mL of the PTB7/chlorobenzene solution and kept in a mechanical agitator for one night. The PTB7/chlorobenzene/SiNCs colloid (1 mL) was then spin-coated on the PEDOT:PSS layer previously deposited on the ITO-coated glass substrates; finally, ~100 nm of aluminum metal was thermally evaporated on the spin-coated film to form the contacts. Current density–voltage (J – V) characterization of the solar cells was measured under AM 1.5G (with Sub Femtoamp Keithley 6430), which was calibrated against a standard a-Si solar cell.

RESULTS AND DISCUSSION

The FTIR spectra of n-type AP- and SE-SiNCs are shown in Figure 1. H-terminations, Si dimers and surface defects are common for electrochemically etched SiNCs.^{26,27,35} In AP-SiNCs, Si–H absorption peaks are observed at 611, 619, 738, 976, and 2073 cm^{-1} . The lower absorption signal of Si–H bending and stretching with back-bond oxidation is found at 877 and 2239 cm^{-1} .^{28,27} These revealed that Si dimers and dangling bonds of the few outer monolayers are likely oxidized when SiNCs are dispersed in ethanol or exposed to humid air (e.g., while drying before measurements).²⁶ After surface engineering, n-type SiNCs are passivated by Si–H_x, Si–O–Si, and O₂SiH₂ bonds. The absorption at 877 cm^{-1} and at 2235 cm^{-1} associated with the back-bond have disappeared and decreased, respectively; this suggests limited inward oxidation in the n-type SE-SiNCs. The absorption peak at 828 cm^{-1} and 1000–1100 cm^{-1} for Si–O–Si is very prominent for both the n-type samples before and after surface engineering (Figure 1), but their shape highlight differing oxide stoichiometry. FTIR for p-type SiNCs was reported and discussed elsewhere,²⁶ where AP- and SE-SiNCs were compared; in this case, a direct-current (DC) microplasma treatment was used for surface engineering; however, we also demonstrated that both DC and RF microplasmas produce the same surface chemistry on SiNCs.³³ p-Type AP-SiNCs have multiple peaks assigned to Si–H_x and Si–O–Si, similarly to n-type AP-SiNCs. P-type SiNCs have H-terminations completely removed and short organic ligand of the type Si–O–R established with a higher quality oxide under-layer.^{19,26}

P-type SiNCs also present a broad OH related absorption between 3000 and 3750 cm^{-1} very likely associated with C–OH groups.²⁶ FTIR of n-type SE-SiNCs, however, does not present this OH absorption. Although the same SE process is applied, it is clear that SiNCs doping has an impact on the surface reactions. The mechanisms leading to these differences are depicted in Figure 2.

The chemical reactions induced at the plasma-liquid interface are still debated in the literature^{26,33,36,37} (see also Supporting Information); however evidence exist that given species are

produced in the liquid phase due to the plasma-induced chemistry. In particular, in this context OH, H₂O₂, and CH₃CH₂O[·] radicals are formed.^{4,26,27,33} p-Type SiNCs can present surface holes, so that negatively charged ions (i.e., CH₃CH₂O[·]) can readily react and replace the Si–H terminations with Si–O–R passivation preventing any further oxidation.²¹ In the case of n-type SiNCs, negatively charged ions will not be reacting with the electron-rich surface of the SiNCs leaving the way to slower reactions with OH and H₂O₂. For instance, the replacement of H-terminations with Si–OH, can then lead to condensation, via (SiOH)₂ → Si₂O + H₂O, and the formation of a surface oxide network of the type Si–O–Si; in the initial stages, hydrogen peroxide and water can also oxidize Si back-bonds and contribute to inward surface oxidation.^{4,27} This analysis is supported by the FTIR spectra presented in Figure 1 and highlights the importance of doping for surface engineering strategies; therefore, chemical functionalization developed for intrinsic SiNCs are expected to produce different results for doped SiNCs and new chemical strategies will need to be devised.

The different surface chemistries induced by the same surface engineering approach on p-type and n-type SiNCs are also evident in the SiNCs optical properties. The PL spectra of n-/p-type AP- and SE-SiNCs are reported in Figure 3 (see also corresponding UV-vis absorption spectra in the Supporting Information). n-Type SiNCs show (Figure 3a) a 26-fold increment shortly after surface engineering, with a 110 nm red-shift of the peak wavelength. However, the high intensity PL of n-type SE-SiNCs is not stable and is subject to a degree of degradation over time; nonetheless, the PL intensity is still twice as high the PL of AP-SiNCs after 7 days (Supporting Information). After surface engineering, the PL intensity of p-type SE-SiNCs increases by a factor of ~9 (Figure 3b) and with a 65 nm red-shift of the peak wavelength. Surface passivation with Si–O–R for p-type SiNCs also enhances the PL stability, which is almost constant and with not much shift in the peak wavelength after 7 days (Supporting Information).²⁶

The PL results are closely related to the surface properties of the SiNCs. The dramatic PL increase for n-type SE-SiNCs is linked to the surface oxidation, which is known to provide radiative recombination paths for excited electron–hole pairs. The surface of small SiNCs plays an important role for their PL spectrum³⁵ and also the surface species and degree/type of oxidation defines the blue or red shifts of the PL.^{38,39} The surface transition from H-passivation to oxygen-based passivation is known to result in the red shift of the photoluminescence peak, where carriers recombination occurs via oxygen-related localized states.^{4,26,35,39–43} The oxide configuration and coordination has also dramatic effects on the extent of the red-shift and for instance larger red-shifts can be determined by a higher degree of oxidation.³⁵ This is also related to the strong electronegativity of oxygen, as the valence electrons from Si atoms are transferred to the oxygen causing a weakening of the nearest neighboring Si–Si bond.

Therefore, p-type SiNCs with Si–O–H or Si–O–C surface terminations present limited coordination of Si–O bonds. From the FTIR results of n-type SE-SiNCs, the absence of Si–O–H/O–C passivation, but an extended Si–O–Si oxide network, leads to a dramatic increment of PL with a marked red-shift. The increased surface concentration of Si–O bonds in n-type SiNCs resulting from the plasma-induced surface chemistry is therefore responsible for the larger red-shift where dopant density also favors tunneling to ionize oxygen

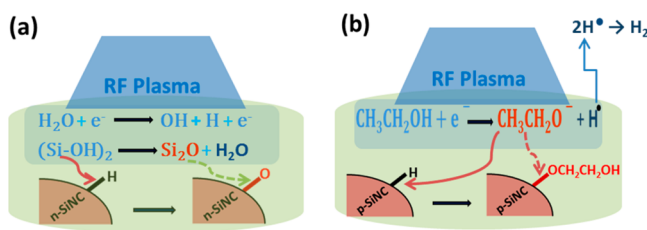


Figure 2. Schematic diagram depicting the dopant-dependent microplasma stimulated surface reactions: (a) n-type silicon nanocrystals (SiNCs) and (b) p-type SiNCs. RF stands for radio frequency.

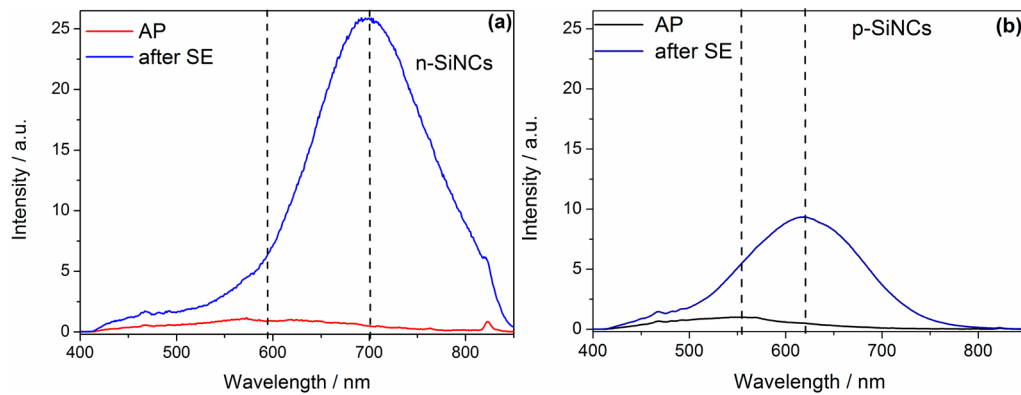


Figure 3. Photoluminescence (PL) spectrum of the as-prepared (AP) and surface engineered (SE) (a) n-type SiNCs and (b) p-type SiNCs in ethanol (PL maxima is denoted by dotted lines in each spectra).

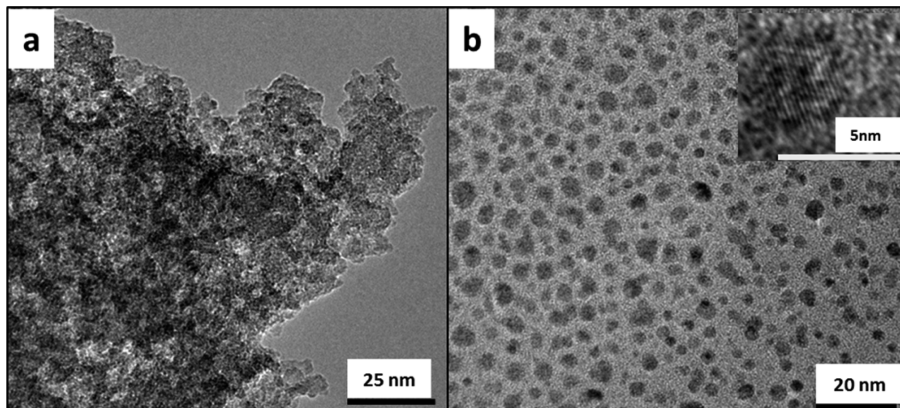


Figure 4. Transmission electron microscopy images of (a) as-prepared and (b) surface engineered n-type silicon nanocrystals (SiNCs); (b, inset) high-resolution TEM image of n-type SiNCs.

atoms and the formation of oxygen-related localized states.⁸ However, over time, back-bond oxidation is not fully prevented in n-type SiNCs, which causes both the formation of strain bonds (resulting in a decreasing PL intensity) and a reduction of the silicon core diameter that results in a gradual blue shift (see Supporting Information for PL after 7 days).^{4,26,39} p-Type SiNCs show a well-passivated surface after SE where the Si–O–R terminations provide both chemical and steric stability (see also Supporting Information for PL spectra after 7 days).

The microplasma processing results not only in the modification of surface characteristics as it also has an effect on the aggregated state of the SiNCs.^{26,27} Transmission electron microscopy (TEM) image of AP and SE n-type SiNCs are shown in Figure 4; this clearly shows that after surface engineering, the SiNCs aggregates are more fragmented and SiNCs are better dispersed. However, while 2–3 nm diameter SiNCs are now clearly visible, some larger aggregates are still present (Figure 4b). Electron-induced electrostatic force may have been responsible for the fragmentation of SiNCs aggregates or through interface passivation.^{26,27}

These SiNCs, due to their size, are expected to present an electron wave function overlapping with the surface states. Therefore, in addition to the optical properties, the band energy structure is expected to be affected by surface engineering schemes. Consequently, we have assessed the Fermi level of SiNCs, deposited as films, by Kelvin Probe measurements. Mapping of the Fermi level (ϕ) with respect to vacuum level for porous films, AP- and SE-SiNCs is shown in

Figure 5. The probe scans the surface of the SiNCs film producing a 2-dimensional map of Fermi level values (note that

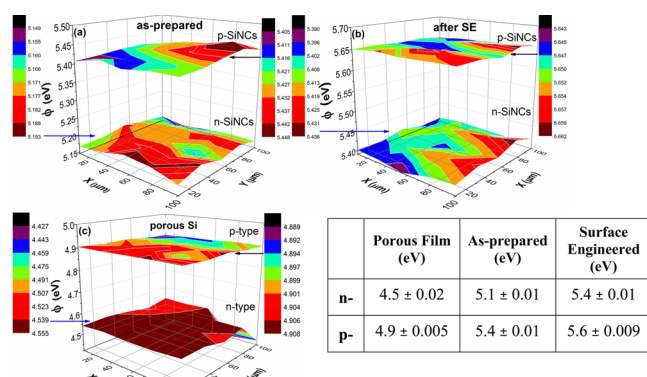


Figure 5. Fermi levels (ϕ) of p-/n-type (a) as-prepared (AP) silicon nanocrystals, (b) surface engineered (SE) silicon nanocrystals, and (c) porous Si film. (Table) Corresponding average ϕ values and respective standard deviations.

absolute values are reported and discussed here below). Local variations are due to intrinsic measurement errors, as well as actual morphological and chemical surface irregularities.

To produce the Fermi level of each sample, we have therefore averaged each corresponding measurement over the scanned surface area; both average values and corresponding

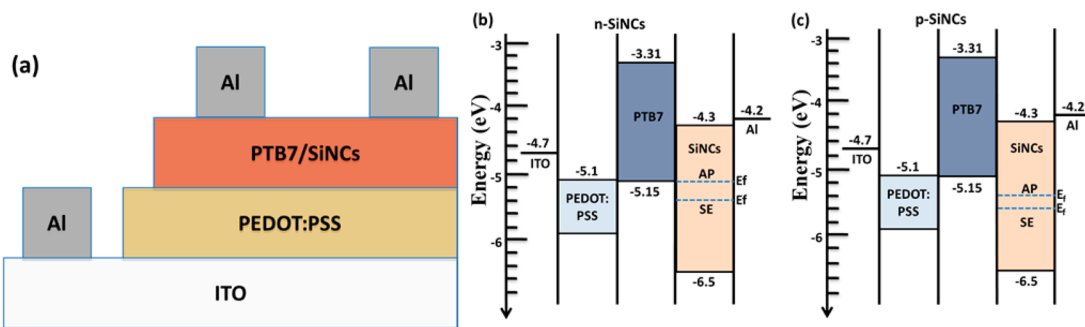


Figure 6. (a) Device structure of the bulk heterojunction and corresponding band alignment for devices with (b) n-type Si nanocrystals (NCs) and (c) p-type Si-NCs. Dotted lines in panels b and c represent the Fermi level value of the as-prepared (AP) and surface engineered (SE) n-/p-SiNCs.

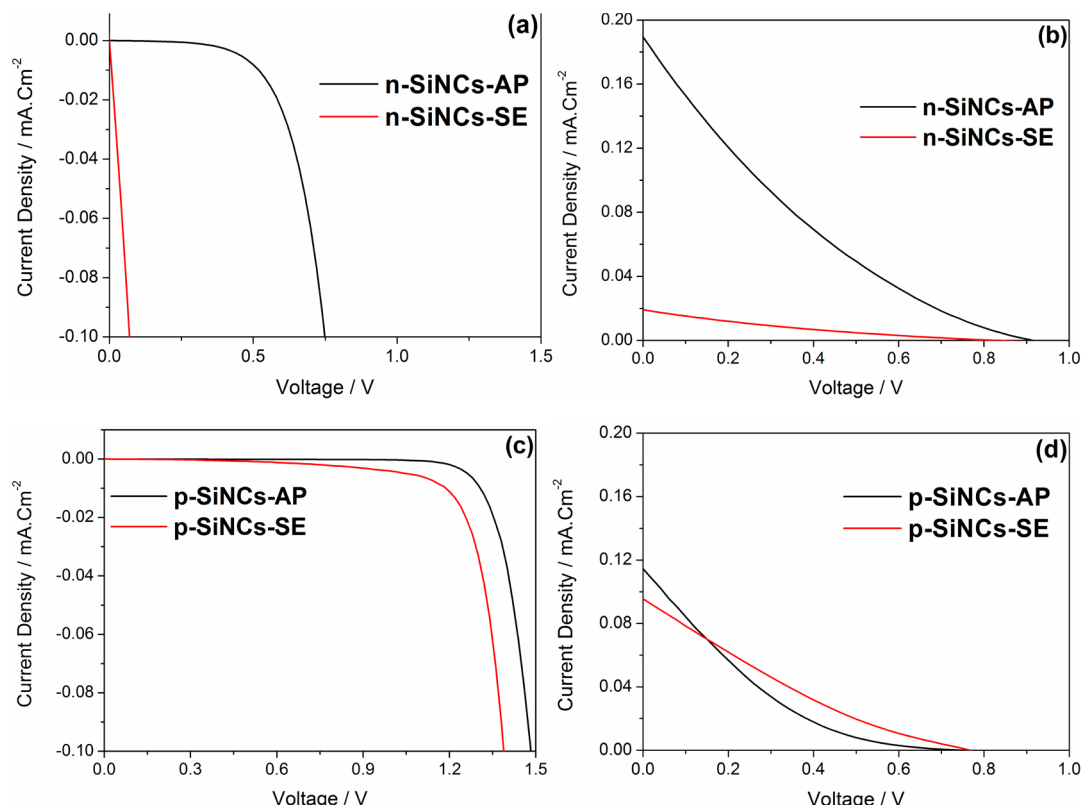


Figure 7. Current density–voltage characteristics of the devices under (a and c) dark or (b and d) AM 1.5G illumination condition with (a and b) n-type Si nanocrystals (NCs) and (c and d) p-type Si NCs.

standard deviations for each sample are reported in the table of Figure 5 (see also Supporting Information and refs 13, 15, and 16 for more details). The average Fermi level for n-type porous Si is 4.5 eV and for AP- and SE-SiNCs it is 5.1 and 5.4 eV, respectively. The measured average ϕ value of p-type porous Si is 4.9 eV, and it is 5.4 and 5.6 eV for corresponding AP- and SE-SiNCs, respectively. The effect of doping is evident in all measurements where the Fermi level (absolute values) is consistently higher for p-type SiNCs compared to n-type SiNCs, as expected. The Fermi levels for all increase with aging (i.e., AP-SiNCs) and after surface engineering. This can be explained in terms of surface oxidation or, in general, the formation of Si–O bonds, which can be viewed as surface dipoles. Due to different electronegativity, electrons will shift from Si toward the oxygen atoms causing the increment of the Fermi level.^{44,45} The Fermi level difference due to aging compared to the porous film is 0.6 and 0.5 eV for n-type and p-

type SiNCs, respectively. Similarly, the Fermi level of SE-SiNCs is higher than the porous film by 0.9 eV (n-type) and 0.7 eV (p-type); therefore, both aging in ethanol and surface engineering produce a larger shift in the Fermi level for the n-type SiNCs which maybe the result of mobile surface electrons contributing to a stronger dipole. As suggested above, variations of the measured Fermi level values over the scanned area are observed. Sadewasser et al. reported that the crystal orientations and grain boundaries (e.g., defects between the grains) also affect the ϕ of the semiconductors,¹³ resulting in fluctuation across the sample area.

To examine further the impact of different surface chemistries due to doping, we have integrated p-type and n-type SiNCs in test PV devices. The structure of the devices and n-/p-type band alignments are depicted in Figure 6a–c, respectively; the active area considered for the measurements is 0.04 cm².

J-V graph measured under dark conditions and under light illumination are shown in Figure 7. All the devices exhibit a rectifying behavior (Figure 7a,c). Open-circuit voltage (V_{OC}) short-circuit current density (J_{SC}) fill factor (FF) and efficiency (η) values from the *J-V* graph are tabulated in Table 1.

Table 1. Open Circuit Voltage, Current Density, Fill Factor, and Efficiency of n-Type and p-Type As-Prepared (AP) or Surface-Engineered (SE) Silicon Nanocrystal (SiNCs) Photovoltaic Devices

	n-type SiNCs		p-type SiNCs	
	AP	SE	AP	SE
open circuit voltage (V)	0.92	0.84	0.72	0.80
current density (mA/cm ²)	0.190	0.019	0.142	0.095
fill factor (FF)	0.05	0.06	0.02	0.06
efficiency (η %)	0.010	0.001	0.002	0.005

Figure 7a,b reports the *J-V* of devices with n-type SiNCs. The corresponding V_{OC} and J_{SC} of devices with AP-SiNCs is 0.92 V and 0.19 mA/cm², respectively; devices with n-type SE-SiNCs exhibit both a lower V_{OC} and a lower J_{SC} , the first is 0.84 V and the second is reduced by a factor of ~10. It is possible that the high quality oxide layer formed during surface engineering has contributed to create a detrimental barrier for effective dissociation and transport. Si-oxide, sufficiently thick, is expected all together to reduce the electron mobility of SiNCs^{46,47} that could result in an unbalanced carrier mobility and consequently in a space charge limited photocurrent.^{48,49} This is sufficient to impact the collection ability of the carriers resulting in a dramatic current reduction and minor losses in the V_{OC} . Figure 7c,d show the *J-V* characteristic of devices produced with p-type SiNCs. In this case both V_{OC} (from 0.72 to 0.8 V) and fill factor are improved. The effect of surface engineering also in this case reduces the short-circuit current, however only by about 0.01 mA/cm². Surface passivation might have also in this case a detrimental effect on the interface interactions, possibly reducing the dissociation efficiency due to the formation of an interface barrier. However, the V_{OC} and fill factor improvements are a clear sign of reduced interface trap states with improved transport properties. The changes in the Fermi level also impact the device performance. n-Type SiNCs with the higher Fermi level closer to that of PTB7 can contribute to carrier generation; however when the Fermi level is lowered in the SiNCs (p-type AP-SiNCs and even more for SE-SiNCs), electron barriers are heightened for electrons formed in SiNCs and the dissociating field at the PTB7/Al junction is also reduced. The analysis above indicates the strong influence of a number of factors in determining device performance parameters, making it difficult to draw definitive conclusions. While the device efficiency is yet too low to extrapolate the overall impact on a high-performing device, the use of such devices as test structures has revealed dramatic effects due to the strong interplay between surface effects and doping. The possibility of manipulating the Fermi level via surface engineering is therefore in this context an important aspect that requires careful attention in the design of fully aligned devices.

CONCLUSION

The surface chemistry plays a crucial role in the optoelectronic properties as demonstrated by related photoluminescence and

quantum yield measurements and supported by FTIR results. We have reported how doping can impact the outcome of surface functionalization schemes and consequently result in dramatic effects on the performance of test photovoltaic devices. Furthermore, we have reported for the first time Kelvin probe measurements on SiNCs aimed to determine experimentally their Fermi level. These measurements have confirmed the p- and n-type character of the respective SiNCs. We have also demonstrated and reported important results that evidence the impact of surface states on the band energy structure and specifically on the Fermi level of the SiNCs. All this was achieved by surface engineering by atmospheric pressure microplasma, which confirms to be a powerful method for surface functionalization of nanoparticles. Overall, we have demonstrated that the same surface engineering, surface functionalization scheme, or both can lead to vastly different results for doped SiNCs. This was evident from the surface chemical composition with clear impact on optical properties, energy band structure, interface interaction, and carrier transport.

ASSOCIATED CONTENT

S Supporting Information

The Supporting Information is available free of charge on the ACS Publications website at DOI: 10.1021/acsami.5b06577.

Stability of PL for n/p-type SiNCs, UV-visible absorption, Size distribution of n-type SiNCs, working principle of Kelvin probe. (PDF)

AUTHOR INFORMATION

Corresponding Author

*E-mail: velusamy-t@email.ulster.ac.uk.

Notes

The authors declare no competing financial interest.

ACKNOWLEDGMENTS

This work was supported by the Leverhulme Trust (award n.IN-2012-136), EPSRC (award n.EP/K022237/1) and InvestNI (award n.PoC-325). TV acknowledges the support of the Ulster University Vice-Chancellor Research Studentship. All the authors also thank the activities of the EU-COST Action (TD1208) which have allowed for fruitful discussion.

REFERENCES

- (1) Svrcek, V.; Dohnalova, K.; Mariotti, D.; Trinh, M.; Limpens, R.; Mitra, S.; Gregorkiewicz, T.; Matsubara, K.; Kondo, M. Dramatic Enhancement of Photoluminescence Quantum Yields for Surface-Engineered Si Nanocrystals within the Solar Spectrum. *Adv. Funct. Mater.* **2013**, *23*, 6051–6058.
- (2) Trinh, M. T.; Limpens, R.; de Boer, W. D. A. M.; Schins, J. M.; Siebbeles, L. D. A.; Gregorkiewicz, T. Direct Generation of Multiple Excitons in Adjacent Silicon Nanocrystals Revealed by Induced Absorption. *Nat. Photonics* **2012**, *6*, 316–321.
- (3) Timmerman, D.; Valenta, J.; Dohnalova, K.; de Boer, W. D. A. M.; Gregorkiewicz, T. Step-like Enhancement of Luminescence Quantum Yield of Silicon Nanocrystals. *Nat. Nanotechnol.* **2011**, *6*, 710–714.
- (4) Mariotti, D.; Mitra, S.; Svrcek, V. Surface-Engineered Silicon Nanocrystals. *Nanoscale* **2012**, *5*, 1385–1398.
- (5) Yu, P.; Tsai, C. Y.; Chang, J. K.; Lai, C. C.; Chen, P. H.; Lai, Y. C.; Tsai, P. T.; Li, M. C.; Pan, H. T.; Huang, Y. Y.; Wu, C. I.; Chueh, Y. L.; Chen, S. W.; Du, C. H.; Horng, S. F.; Meng, H. F. 13%

- Efficiency Hybrid Organic/Silicon-Nanowire Heterojunction Solar Cell via Interface Engineering. *ACS Nano* **2013**, *7*, 10780–10787.
- (6) Zhong, S.; Huang, Z.; Lin, X.; Zeng, Y.; Ma, Y.; Shen, W. High-Efficiency Nanostructured Silicon Solar Cells on a Large Scale Realized Through the Suppression of Recombination Channels. *Adv. Mater.* **2015**, *27*, 555–561.
- (7) Milliron, D. J. Quantum Dot Solar Cells: The Surface Plays a Core Role. *Nat. Mater.* **2014**, *13*, 772–773.
- (8) Zhou, S.; Pi, X.; Ni, Z.; Luan, Q.; Jiang, Y.; Jin, C.; Nozaki, T.; Yang, D. Boron- and Phosphorus-Hyperdoped Silicon Nanocrystals. *Part. Part. Syst. Charact.* **2015**, *32*, 213–221.
- (9) Pi, X. D.; Gresback, R.; Liptak, R. W.; Campbell, S. A.; Kortshagen, U. Doping Efficiency, Dopant Location, and Oxidation of Si Nanocrystals. *Appl. Phys. Lett.* **2008**, *92*, 123102–123104.
- (10) Wheeler, L. M.; Neale, N. R.; Chen, T.; Kortshagen, U. R. Hypervalent Surface Interactions for Colloidal Stability and Doping of Silicon Nanocrystals. *Nat. Commun.* **2013**, *4*, 2197–2206.
- (11) Gresback, R.; Kramer, N. J.; Ding, Y.; Chen, T.; Kortshagen, U. R.; Nozaki, T. Controlled Doping of Silicon Nanocrystals Investigated by Solution-Processed Field Effect Transistors. *ACS Nano* **2014**, *8*, S650–S656.
- (12) Ishii, H.; Sugiyama, K.; Ito, E.; Seki, K. Energy Level Alignment and Interfacial Electronic Structures at Organic/Metal and Organic/Organic Interfaces. *Adv. Mater.* **1999**, *11*, 605–625.
- (13) Sadewasser, S.; Glatzel, Th.; Rusu, M.; Jager-Waldau, A.; Lux-Steiner, M. Ch. High-Resolution Work Function Imaging of Single Grains of Semiconductor Surfaces. *Appl. Phys. Lett.* **2002**, *80*, 2979–2981.
- (14) Chuang, C. H. M.; Brown, P. R.; Bulovic, V.; Bawendi, M. G. Improved Performance and Stability in Quantum Dot Solar Cells Through Band Alignment Engineering. *Nat. Mater.* **2014**, *13*, 796–801.
- (15) Nonnenmacher, M.; O’Boyle, M. P.; Wickramasinghe, H. K. Kelvin Probe Force Microscopy. *Appl. Phys. Lett.* **1991**, *58*, 2921–2923.
- (16) Glatzel, Th.; Sadewasser, S.; Shikler, R.; Rosenwaks, Y.; Lux-Steiner, M. Ch. Kelvin Probe Force Microscopy on III/V Semiconductors: The Effect of Surface Defects on the Local Work Function. *Mater. Sci. Eng., B* **2003**, *102*, 138–142.
- (17) Greiner, M. T.; Chai, L.; Helander, M. G.; Tang, W. M.; Lu, Z. H. Transition Metal Oxide Work Functions: The Influence of Cation Oxidation State and Oxygen Vacancies. *Adv. Funct. Mater.* **2012**, *22*, 4557–4568.
- (18) Nozik, A. J. Nanoscience and Nanostructures for Photovoltaics and Solar Fuels. *Nano Lett.* **2010**, *10*, 2735–2741.
- (19) Svrcek, V.; Mariotti, D.; Kondo, M. Microplasma-Induced Surface Engineering of Silicon Nanocrystals in Colloidal Dispersion. *Appl. Phys. Lett.* **2010**, *97*, 161502–161504.
- (20) Svrcek, V.; Fujiwara, H.; Kondo, M. Improved Transport and Photostability of poly(methoxy-ethoxyloxy-phenylenevinylene) Polymer Thin Films by Boron Doped Freestanding Silicon Nanocrystals. *Appl. Phys. Lett.* **2008**, *92*, 143301–143303.
- (21) Yu, G.; Gao, J.; Hummelen, J. C.; Wudl, F.; Heeger, A. J. Polymer Photovoltaic Cells: Enhanced Efficiencies via a Network of Internal Donor-Acceptor Heterojunctions. *Science* **1995**, *270*, 1789–1791.
- (22) Oosterhout, S. D.; Koster, L. J. A.; van Bavel, S. S.; Loos, J.; Stenzel, O.; Thiedmann, R.; Schmidt, V.; Campo, B.; Cleij, T. J.; Lutzen, L.; Vanderzande, D.; Wienk, M. M.; Janssen, R. A. J. Controlling the Morphology and Efficiency of Hybrid ZnO:Polythiophene Solar Cells Via Side Chain Functionalization. *Adv. Energy Mater.* **2011**, *1*, 90–96.
- (23) Holman, Z. C.; Kortshagen, U. R. Nanocrystal Inks without Ligands: Stable Colloids of Bare Germanium Nanocrystals. *Nano Lett.* **2011**, *11*, 2133–2136.
- (24) Van Buuren, T.; Dinh, L.; Chase, L. L.; Siekhaus, W.; Terminello, L. J. Changes in the Electronic Properties of Si Nanocrystals as a Function of Particle Size. *Phys. Rev. Lett.* **1998**, *80*, 3803–3806.
- (25) Semonin, O. E.; Luther, J. M.; Choi, S.; Chen, H. Y.; Gao, J.; Nozik, A. J.; Beard, M. C. Peak External Photocurrent Quantum Efficiency Exceeding 100% via MEG in a Quantum Dot Solar Cell. *Science* **2011**, *334*, 1530–1533.
- (26) Mariotti, D.; Svrcek, V.; Hamilton, J. W. J.; Schmidt, M.; Kondo, M. Silicon Nanocrystals in Liquid Media: Optical Properties and Surface Stabilization by Microplasma-Induced Non-Equilibrium Liquid Chemistry. *Adv. Funct. Mater.* **2012**, *22*, 954–964.
- (27) Mitra, S.; Cook, S.; Svrcek, V.; Blackley, R. A.; Zhou, W.; Kovac, J.; Cvelbar, U.; Mariotti, D. Improved Optoelectronic Properties of Silicon Nanocrystals/Polymer Nanocomposites by Microplasma-Induced Liquid Chemistry. *J. Phys. Chem. C* **2013**, *117*, 23198–23207.
- (28) International Technology Roadmap for Photovoltaic (ITRPV), SEMI PV Group Europe, 2013, <http://www.itrpv.net/> (Revision 1, 24 March 2014).
- (29) ur Rehman, A.; Lee, S. H. Advancements in n-Type Base Crystalline Silicon Solar Cells and Their Emergence in the Photovoltaic Industry. *Sci. World J.* **2013**, *2013*, 470347.
- (30) Macdonald, D.; Geerligs, L. J. Recombination Activity of Interstitial Iron and Other Transition Metal Point Defects in p-and n-type Crystalline Silicon. *Appl. Phys. Lett.* **2004**, *85*, 4061–4063.
- (31) Svrcek, V.; Mariotti, D.; Mitra, S.; Kaneko, T.; Li, L.; Cvelbar, U.; Matsubara, K.; Kondo, M. Built-In Charges and Photoluminescence Stability of 3D Surface-Engineered Silicon Nanocrystals by a Nanosecond Laser and a Direct Current Microplasma. *J. Phys. Chem. C* **2013**, *117*, 10939–10948.
- (32) Spallino, L.; Vaccaro, L.; Sciotino, L.; Agnello, S.; Buscarino, G.; Cannas, M.; Gelardi, F. M. Visible-Ultraviolet Vibronic Emission of Silica Nanoparticles. *Phys. Chem. Chem. Phys.* **2014**, *16*, 22028–22034.
- (33) Mitra, S.; Svrcek, V.; Mariotti, D.; Velusamy, T.; Matsubara, K.; Kondo, M. Microplasma-Induced Liquid Chemistry for Stabilizing of Silicon Nanocrystals Optical Properties in Water. *Plasma Processes Polym.* **2014**, *11*, 158–163.
- (34) Svrcek, V.; Mariotti, D.; Nagai, T.; Shibata, Y.; Turkevych, I.; Kondo, M. Photovoltaic Applications of Silicon Nanocrystal Based Nanostructures Induced by Nanosecond Laser Fragmentation in Liquid Media. *J. Phys. Chem. C* **2011**, *115*, 5084–5093.
- (35) Wolkin, M.; Jorne, J.; Fauchet, P.; Allan, G.; Delerue, C. Electronic States and Luminescence in Porous Silicon Quantum Dots: The Role of Oxygen. *Phys. Rev. Lett.* **1999**, *82*, 197–200.
- (36) Patel, J.; Némcová, L.; Maguire, P.; Graham, W. G.; Mariotti, D. Synthesis of Surfactant-Free Electrostatically Stabilized Gold Nanoparticles by Plasma-Induced Liquid Chemistry. *Nanotechnology* **2013**, *24*, 245604–245614.
- (37) Bruggeman, P.; Schram, D. C. On OH Production in Water Containing Atmospheric Pressure Plasmas. *Plasma Sources Sci. Technol.* **2010**, *19*, 045025–045033.
- (38) Kelly, J. A.; Veinot, J. G. C. An Investigation into Near-UV Hydrosilylation of Freestanding Silicon Nanocrystals. *ACS Nano* **2010**, *4*, 4645–4656.
- (39) Chen, X. B.; Pi, X. D.; Yang, D. R. Bonding of Oxygen at the Oxide/Nanocrystal Interface of Oxidized Silicon Nanocrystals: An Ab Initio Study. *J. Phys. Chem. C* **2010**, *114*, 8774–8781.
- (40) Shu, Y.; Levine, B. G. Non-Radiative Recombination via Conical Intersections Arising at Defects on the Oxidized Silicon Surface. *J. Phys. Chem. C* **2015**, *119*, 1737–1747.
- (41) Rodríguez Núñez, J. R.; Kelly, J. A.; Henderson, E. J.; Veinot, J. G. C. Wavelength-Controlled Etching of Silicon Nanocrystals. *Chem. Mater.* **2012**, *24*, 346–352.
- (42) Fuzell, J.; Thibert, A.; Atkins, T. M.; Dasog, M.; Busby, E.; Veinot, J. G. C.; Kauzlarich, S. M.; Larsen, D. S. Red States versus Blue States in Colloidal Silicon Nanocrystals: Exciton Sequestration into Low-Density Traps. *J. Phys. Chem. Lett.* **2013**, *4*, 3806–3812.
- (43) Zhou, Z. Y.; Brus, L.; Friesner, R. Electronic Structure and Luminescence of 1.1- and 1.4-nm Silicon Nanocrystals: Oxide Shell Versus Hydrogen Passivation. *Nano Lett.* **2003**, *3*, 163–167.
- (44) Petermann, U.; Baikie, I. D.; Lagel, B. Kelvin Probe Study of Metastable States During Initial Oxygen Adsorption Dynamics on Si (111) 7 × 7. *Thin Solid Films* **1999**, *344*, 492–494.

- (45) Raisin, C.; Vieujot-Testemale, E.; Brahim, A. B.; Palau, J. M.; Lassabatere, L. Work Function Measurements During Growth of Ultra Thin Films of SiO₂ on Characterized Silicon Surfaces. *Solid-State Electron.* **1984**, *27*, 413–417.
- (46) Ding, Y.; Gresback, R.; Liu, Q.; Zhou, S.; Pi, X.; Nozaki, T. Silicon Nanocrystal Conjugated Polymer Hybrid Solar Cells with Improved Performance. *Nano Energy* **2014**, *9*, 25–31.
- (47) Ding, Y.; Sugaya, M.; Liu, Q.; Zhou, S.; Nozaki, T. Oxygen Passivation of Silicon Nanocrystals: Influences on Trap states, Electron mobility, and Hybrid Solar Cell Performance. *Nano Energy* **2014**, *10*, 322–328.
- (48) Li, G.; Shrotriya, V.; Huang, J.; Yao, Y.; Moriarty, T.; Emery, K.; Yang, Y. High-Efficiency Solution Processable Polymer Photovoltaic Cells by Self-Organization of Polymer Blends. *Nat. Mater.* **2005**, *4*, 864–868.
- (49) Blom, P. W.; Mihailescu, V. D.; Koster, L. J. A.; Markov, D. E. Device Physics of Polymer:Fullerene Bulk Heterojunction Solar Cells. *Adv. Mater.* **2007**, *19*, 1551–1556.